Stem Cell Reports
Resource
ISSCR
OPEN ACCESS

Aggregation of cryopreserved mid-hindgut endoderm for more reliable and reproducible hPSC-derived small intestinal organoid generation

Amy L. Pitstick,[1,2,5] Holly M. Poling,[3,5] Nambirajan Sundaram,[3,5] Phillip L. Lewis,[2,5] Daniel O. Kechele,[2,5] J. Guillermo Sanchez,[2,5] Melissa A. Scott,[5] Taylor R. Broda,[2,5] Michael A. Helmrath,[2,5] James M. Wells,[2,4,5] and Christopher N. Mayhew[2,5,*]
[1]Department of Pediatrics, University of Cincinnati College of Medicine, Cincinnati, OH, USA
[2]Division of Developmental Biology, Cincinnati Children's Hospital Medical Center, 3333 Burnet Avenue, Cincinnati, OH 45229, USA
[3]Division of Pediatric General and Thoracic Surgery, Cincinnati Children's Hospital Medical Center, 3333 Burnet Avenue, Cincinnati, OH 45229, USA
[4]Division of Endocrinology, Cincinnati Children's Hospital Medical Center, 3333 Burnet Avenue, Cincinnati, OH 45229, USA
[5]Center for Stem Cell and Organoid Medicine, Cincinnati Children's Hospital Medical Center, 3333 Burnet Avenue, Cincinnati, OH 45229, USA
*Correspondence: christopher.mayhew@cchmc.org
https://doi.org/10.1016/j.stemcr.2022.06.011

SUMMARY

A major technical limitation hindering the widespread adoption of human pluripotent stem cell (hPSC)-derived gastrointestinal (GI) organoid technologies is the need for *de novo* hPSC differentiation and dependence on spontaneous morphogenesis to produce detached spheroids. Here, we report a method for simple, reproducible, and scalable production of small intestinal organoids (HIOs) based on the aggregation of cryopreservable hPSC-derived mid-hindgut endoderm (MHE) monolayers. MHE aggregation eliminates variability in spontaneous spheroid production and generates HIOs that are comparable to those arising spontaneously. With a minor modification to the protocol, MHE can be cryopreserved, thawed, and aggregated, facilitating HIO production without *de novo* hPSC differentiation. Finally, aggregation can also be used to generate antral stomach organoids and colonic organoids. This improved method removes significant barriers to the implementation and successful use of hPSC-derived GI organoid technologies and provides a framework for improved dissemination and increased scalability of GI organoid production.

INTRODUCTION

Human pluripotent stem cell (hPSC)-derived organoids provide new opportunities to study human development, homeostasis, and disease (Kim et al., 2020). Organoids recapitulate many of the complexities of multiple cell types organized into 3-dimensional (3D) tissue architecture and represent a more physiologically relevant platform for study. Methods for the generation of hPSC-derived small intestinal organoids (HIOs) were first described in 2011 (Spence et al., 2011) and have been used for studying human development (Du et al., 2012), modeling genetic intestinal disease (Merkert et al., 2019; Sommer et al., 2018), studying enteric pathogenesis (Forbester et al., 2015; Leslie et al., 2015; Son et al., 2020), and identifying mechanisms of intestinal physiology (McCauley et al., 2020).

The production of hPSC-derived HIOs relies on the stepwise differentiation to definitive endoderm (DE), and then to mid-hindgut endoderm (MHE). During MHE differentiation, spontaneous morphogenesis occurs, producing MHE spheroids that detach from the monolayer. These MHE spheroids are collected and embedded in semi-solid extracellular matrix (e.g., Matrigel), after which they undergo growth and cytodifferentiation into HIOs, containing all major fetal intestinal cell types organized into epithelial and mesenchymal layers (Spence et al., 2011). In our experience, the major bottleneck in producing HIOs is the spontaneous spheroid generation step. This is true even when cultures are maintained by experienced technical staff using hPSC lines known to have the ability to produce HIOs. There is also the clone-to-clone and donor-to-donor variability in HIO generation that has profoundly affected other differentiation protocols (Ortmann and Vallier, 2017). A second barrier for adopting any hPSC technology is the requirement for expensive and labor-intensive maintenance of high-quality hPSC cultures and *de novo* generation of HIOs for each application. These obstacles prevent many potential users from adopting hPSC-based organoid technologies.

hPSC-derived progenitor cells can be aggregated to elicit self-organization and subsequent organoid formation (Hannan et al., 2013; Kumar et al., 2019; Takebe et al., 2017). Potentially significant advantages of this approach include (1) bypassing the reliance on the highly variable spontaneous spheroid production and detachment step during the early stages of organoid formation, and (2) the potential for progenitors to be cryopreserved before aggregation and organoid formation, facilitating the production of banks of organoid precursors that can be accessed without maintaining hPSCs in culture. Several studies have reported utilization of the patterned MHE monolayer to generate HIOs (Forbester et al., 2015; Onozato et al., 2018, 2021; Yoshida et al., 2020). However, none of these studies compared the resulting HIOs to those arising spontaneously from multiple hPSC lines, investigated whether MHE can be cryopreserved, banked, and thawed for subsequent HIO generation, nor translated forced aggregation more broadly to other

This is an open access article under the CC BY-NC-ND license (http://creativecommons.org/licenses/by-nc-nd/4.0/).

gastrointestinal (GI) organoid types. Therefore, in this study, we evaluated the ability of aggregated MHE from several hPSC lines to generate HIOs in commercially available micro-aggregation plates (Aggrewell 400; StemCell Technologies), tested whether MHE can be cryopreserved before aggregation and HIO production, and assessed whether additional GI organoid types can be generated by aggregation. We show that MHE derived from all hPSC lines tested, including from cultures in which no spontaneously detached spheroids develop, can be aggregated into spheroids. Following embedding in Matrigel, spheroids undergo stereotypical growth and cytodifferentiation into HIOs that are comparable to those generated from spontaneous spheroids. Critically, MHE monolayers can be cryopreserved as single cells and subsequently thawed and, with a minor modification to the protocol, aggregated to produce HIOs, facilitating the production of quality controlled MHE that can be stored indefinitely and used for reliable HIO production as needed. Finally, we also demonstrate that the aggregation-based methods for generating HIOs can be used to produce both antral gastric and colonic organoids, indicating the wider applicability for scalable production of GI organoids. Collectively, our data provide an improved protocol for HIO production that will significantly enhance access to and dissemination of these technologies and improve the reproducibility of GI organoid production for both basic science and translational applications.

RESULTS

Variability in spontaneous spheroid production and detachment

Current protocols for the directed differentiation of hPSCs to HIOs (Figure 1A) rely on spontaneous morphogenesis, the self-organization of cells into primitive gut tube-like 3D spheroids during patterning of MHE monolayers. Spheroids that detach are embedded in Matrigel for maturation into HIOs (McCracken et al., 2011; Spence et al., 2011). We have quantitatively shown that following the differentiation of hPSCs plated as cell clusters, the production of detached spheroids is the rate-limiting step in this protocol, manifested by either no/poor spontaneous morphogenesis or failure of spheroid detachment or both. In 140 experiments set up by a single individual (A.L.P.) using H1 hESCs (8 wells of a 24-well cell culture dish per experiment), robust spheroid detachment (average >50 detached spheroids per well of a 24-well plate) was observed in only 54% of experiments, 10% of experiments resulted in limited spheroid detachment (average <50 detached spheroids per well), and 36% produced no detached spheroids at all (data not shown). Furthermore, we observed line-to-line differences in detached spheroid production (Figures 1B and 1C) from 4 well-characterized hESC and iPSC lines (Figure S1). Lastly, we also noted well-to-well variability in the detachment of MHE spheroids (Figure 1D). In most cases in which detached spheroids did not form, we still observed morphogenesis of the monolayer. However, in some cases, MHE had limited or no spontaneous morphogenesis. We further assessed cell seeding density effects as previously observed (Chambers et al., 2009; Wilson et al., 2015), but seeding density was consistent (Figure S2A) and did not correlate with the variability. Indeed, hPSCs plated as single cells were similarly subject to significant variability in the production of detached spheroids (Figure S2B). Finally, all lines demonstrated endoderm potential in Scorecard assays (Figure S1D) and generated DE efficiently in directed differentiation assays (data not shown), indicating that differences in DE potential do not underlie the variability in spheroid production. Collectively, these data indicate that the original HIO protocol suffers from (1) inter-experimental variability using the same hPSC line, (2) hPSC line-to-line variability in spheroid detachment, (3) intra-experimental variability, (4) robust morphogenesis without spheroid detachment, and (5) occasionally complete failure of morphogenesis.

Deficits in spheroid formation are not due to DE differentiation or patterning

To probe the potential mechanism underlying the variability in spontaneous spheroid detachment, we investigated whether earlier stages in differentiation were suboptimal. Immunofluorescence analysis of induction of SOX17/FOXA2 double-positive cells on day 3 of differentiation was similar in all cultures (data not shown), indicating robust DE formation. Therefore, we next analyzed the subsequent patterning of DE to MHE by evaluating the expression of the mid-/hindgut marker CDX2 in day 7 MHE monolayers. Strikingly, we found that MHE monolayers were uniformly positive for CDX2 (Figure 2) and negative for the foregut marker SOX2 (data not shown). This was also true when undifferentiated hPSCs were plated as single cells (Figure S2C). Furthermore, the robust induction of hindgut patterning in MHE cultures was independent of the extent of morphogenesis and spontaneous spheroid production and detachment as even cultures exhibiting poor morphogenesis and no detached spheroids were uniformly $CDX2^+$ (Figures S2E and S2F). These data indicate that qualitative differences in mid-hindgut identity do not underlie the observed variability.

Efficient production of uniform MHE spheroids by micro-aggregation

Due to the unidentifiable nature of the inherent variability of spheroid production, we explored new strategies to generate spheroids. Several studies have shown that the

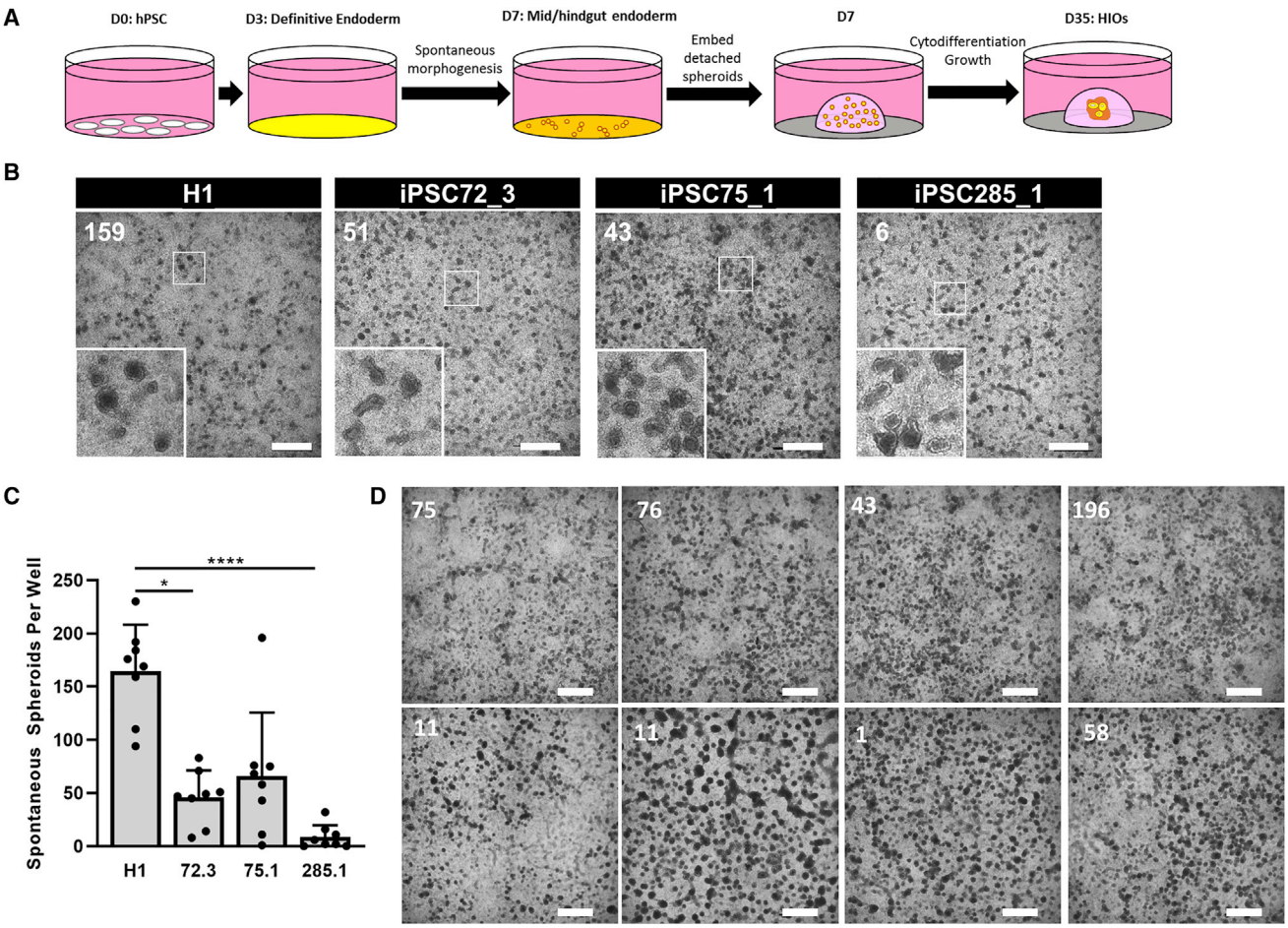

Figure 1. Variability in spontaneous morphogenesis and mid-hindgut endoderm (MHE) spheroid production and detachment

(A) Schematic overview of existing protocol for HIO generation (Spence et al.).

(B) Representative images of morphogenesis at day 7 of differentiation of 4 hPSC lines to MHE (H1 hESCs, iPSC72_3, iPSC75_1, and iPSC285_1). The number of detached spheroids in each well is indicated in white. Scale bar, 1 mm. Inset: Increased magnification of boxed region showing stereotypical morphology of spont-spheroids.

(C) Four hPSC lines were simultaneously plated and differentiated to MHE. The number of detached spontaneously generated spheroids per well in each plate was quantified. Means ± SDs n = 8 wells, *$p < 0.05$; ****$p < 0.0001$.

(D) iPSC75_1 cells were differentiated to day 7 MHE. An image of the representative morphogenesis in each well was captured and the number of detached spontaneously arising spheroids was scored (indicated in white). Scale bar, 1 mm.

aggregation of patterned hPSC-derived cells can be used in the production of organoids (Kumar et al., 2019; Onozato et al., 2018; Takebe et al., 2017). Because MHE differentiation was uniform in all of the cultures examined, even in the absence of spontaneous spheroid formation, we next sought to determine whether the aggregation of day 7 MHE monolayers generates HIOs comparable to those arising from spontaneous morphogenesis at day 7 in the same experiment (Figure 3A). For MHE aggregation, we chose commercially available Aggrewell 400 plates containing 1,200 × 400-μm microwells per well of a 24-well plate and have been used extensively for the formation of embryoid bodies from hPSCs (Kokkinaki et al., 2011; Ungrin et al., 2008). A single-cell suspension of day 7 MHE was prepared from H1 and iPSCs and plated at 3,000 cells per microwell in an Aggrewell 400 plate. Following centrifugation and culture overnight in HIO media, microwells contained uniform aggregates (hereafter referred to as agg-spheroids) with an approximate diameter of 100 μm (Figures 3B and S3A). Compared to spontaneous MHE spheroids (spont-spheroids), the size distribution of H1 agg-spheroids was significantly more homogeneous (Figures 3C and S2B–S2D). MHE aggregation was highly reproducible with robust agg-spheroid production from all of the MHE monolayers tested. Counting spont-spheroids and agg-spheroids produced from the same plate demonstrated that agg-spheroid

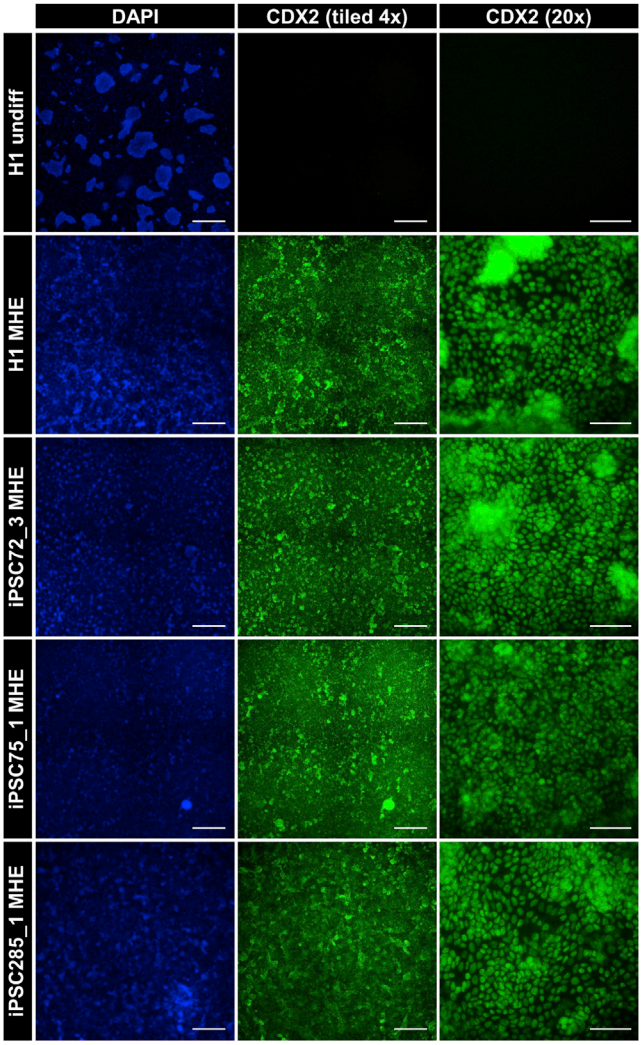

Figure 2. hPSC-derived MHE exhibits uniform hindgut patterning

hPSCs: H1, iPSC72_3, iPSC75_1, and iPSC285_1 were differentiated to day 7 MHE and immunostained with antibodies to the MHE marker CDX2 (green). Cells were counterstained with DAPI (blue). Undifferentiated H1 hESCs served as a CDX2^{-} control. Center panel: Representative tiled 4× images of CDX2 immunostaining in 4 randomly selected adjacent fields (scale bar, 1 mm). Right panel: representative 20× images of CDX2 immunostaining (scale bars, 100 μm).

production was consistently 10- to 20-fold higher than spont-spheroids (Figure 3D). These data demonstrate that MHE monolayers, regardless of the efficiency of spontaneous morphogenesis, can be effectively aggregated to form homogeneous spheroids.

Agg-spheroids retain intestinal identity after embedding in Matrigel

We next compared the development of HIOs made from aggregated MHE or spontaneous spheroids. On differentiation day 7 of H1 hESCs, detached spont-spheroids were harvested and fixed. The remaining monolayers were aggregated and 16 h later, the resulting agg-spheroids were harvested and fixed. Spont- and agg-spheroids were then subjected to whole-mount immunostaining for epithelial markers CDX2 and CDH1 and mesenchymal marker FOXF1. All of the cells in both spont- and agg-spheroids expressed CDX2 and/or FOXF1. However, spont-spheroids consisted of a CDX2^{high}/CDH1^{+} epithelial layer on the outside and a CDX2^{low}/FOXF1^{+} mesenchymal layer in the center of each spheroid (Figure 4A). In contrast, presumably due to the consequences of forced aggregation versus self-organization, FOXF1^{+} mesenchymal cells were located at the periphery of agg-spheroids and colocalized with strong CDX2 expression. Because agg-spheroids appeared to be patterned appropriately, we next embedded spont-spheroids and agg-spheroids in Matrigel to assess their development into HIOs. Despite the differential cellular organization at the time of embedding, after 3 days in Matrigel, H1-derived spont-spheroids and agg-spheroids were morphologically similar to one another, exhibiting an epithelium and a mesenchymal cell population migrating into the Matrigel (Figure 4B). The same morphological characteristics were also noted following the embedding of spont-spheroids and agg-spheroids derived from discrete iPSC lines (Figure S4A). After 3 days in Matrigel, both spont- and agg-spheroids exhibited a CDX2^{+}/CDH1^{+} epithelial layer surrounding a central lumen surrounded by FOXF1^{+} mesenchymal cells (Figure 4C). Together, these data demonstrate that while initially organized differently, agg-spheroids appear to retain responsiveness to critical factors in Matrigel that promote morphogenesis, and epithelial and mesenchymal cells rapidly reorganize to become comparable to spont-spheroids.

Agg-HIOs are morphologically and histologically similar to spont-HIOs

In standard protocols, *in vitro* growth and cytodifferentiation of spheroids into HIOs occurs over ~28 days following embedding in Matrigel (day 35 from start of PSC differentiation) (McCracken et al., 2011; Spence et al., 2011). Therefore, we next compared the growth and morphology of spont- and agg-spheroids developing into day 35 HIOs. No differences in the gross morphology of developing organoids were detected. Whether derived from spont-spheroids or agg-spheroids generated from hPSCs plated as either clusters or single cells, the size and morphology of developing organoids (hereafter referred to as spont-HIOs and agg-HIOs) were similar, containing convoluted epithelial layers surrounded by mesenchyme (Figures 5A, S2D, and S4B). Analysis of CDH1 and EMILIN1 demonstrated the formation of a pseudostratified epithelia expressing CDX2^{+}, PDX1^{+}, and CDH17^{+}, confirming small intestinal identity

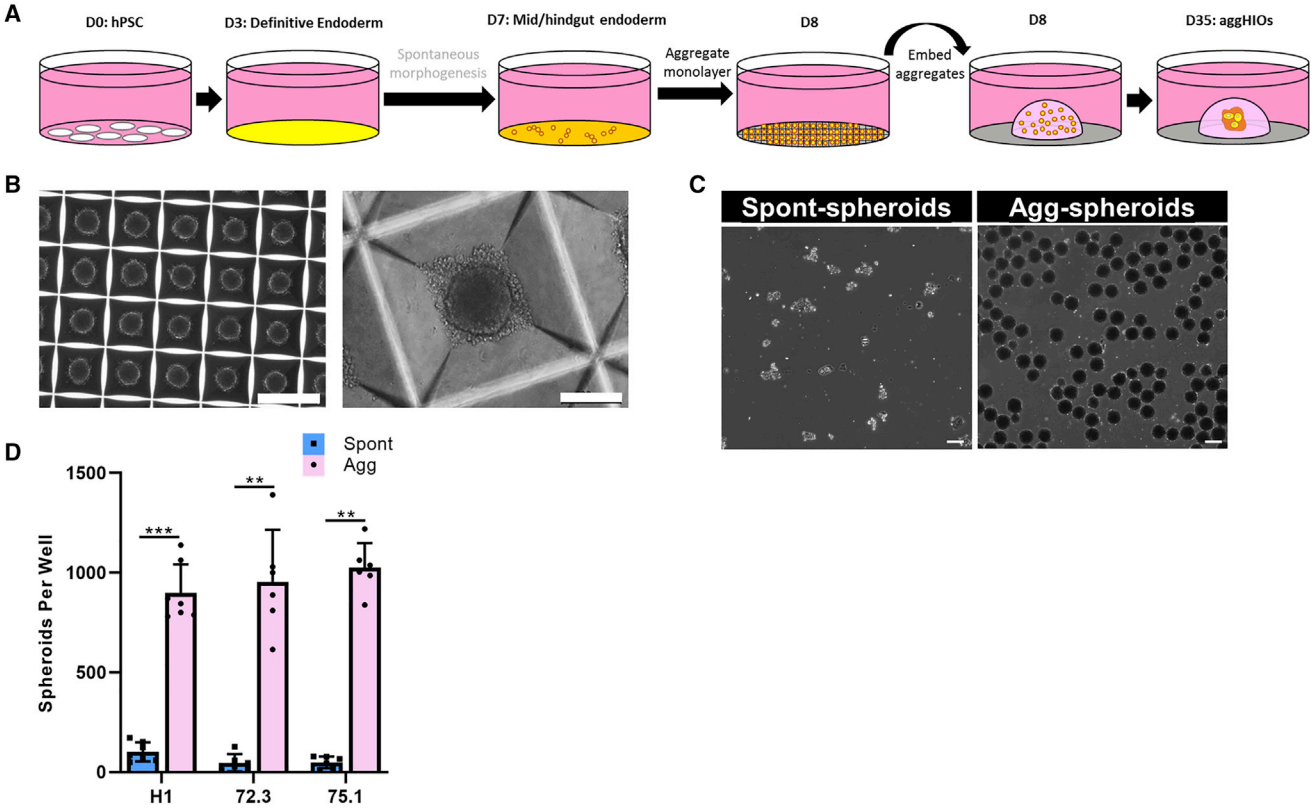

Figure 3. Robust and uniform aggregation of mid-/hindgut endoderm

(A) Schematic overview of improved HIO generation protocol incorporating aggregation of MHE on day 7 for agg-spheroid production.
(B) Representative images of aggregates were captured 16 h after plating MHE (left panel scale bar, 500 μm; right panel scale bar, 100 μm).
(C) H1 cells were differentiated to day 7 MHE and spont-spheroids were harvested. The remaining monolayer was aggregated (agg-spheroids) and harvested at day 8. Spont- and agg-spheroids were imaged using a Keyence BZ-X710 imaging system. Scale bar, 100 μm.
(D) H1, iPSC72_3, and iPSC75_1 cells were each differentiated to day 7 MHE. Detached spont-spheroids were removed and counted. Monolayer cells were aggregated and counted. Mean spont- and agg-spheroid production (±SD) per well is shown (n = 6–8 experiments). Statistical significance was assessed using a non-parametric Mann-Whitney test, where $^{**}p \leq 0.003$ and $^{***}p < 0.001$.

(Figures 5B and 5C). Compared to spont- and agg-spheroids, TaqMan qRT-PCR analysis of day 35 HIOs demonstrated the robust induction of OLMF4 and LGR5 (intestinal epithelial stem cells), as well as intestinal epithelial differentiation markers LYZ (Paneth cells), DPP4 (enterocytes), MUC2 (goblet cells), and CHGA (chromogranin A; enteroendocrine cells; Figure S4C). No significant difference in the expression of these genes between spont-HIOs and agg-HIOs was detected. Finally, epithelial expression of DPP4, MUC2, and CHGA at the protein level was confirmed in both spont- and agg-HIOs (Figures 5D and S4D).

To determine whether MHE aggregation could alleviate the significant variability in spontaneous spheroid production, we used an iPSC line (iPSC115_1) that was inefficient in spont-spheroid production. We also chose an experiment in which MHE morphogenesis was poor and no detached spont-spheroids formed (Figure S2E). MHE monolayers from this experiment were uniformly patterned to $CDX2^+$ and $SOX2^-$ MHE (Figure S2F) and could be aggregated in Aggrewell 400 plates (Figure S2G). Critically, 35 days after embedding agg-spheroids in Matrigel, organoids contained $CDH1^+/CDX2^+/CDH17^+$ intestinal epithelia surrounded by a layer of $EMILIN1^+$ mesenchyme (Figure S2H), demonstrating effective production of agg-HIOs from MHE monolayers that exhibited failed morphogenesis and spont-spheroid production.

Growth and maturation of agg-HIOs following transplantation into mice

Transplantation of spont-HIOs into the kidney capsule or mesentery of immunodeficient mice results in vascularization and significant growth and development of mature small intestine-like organoids (Cortez et al., 2018; Watson et al., 2014). This is the gold standard method to show the quality of HIOs generated *in vitro*. Therefore, to assess *in vivo* maturation of agg-HIOs, we transplanted agg-HIOs

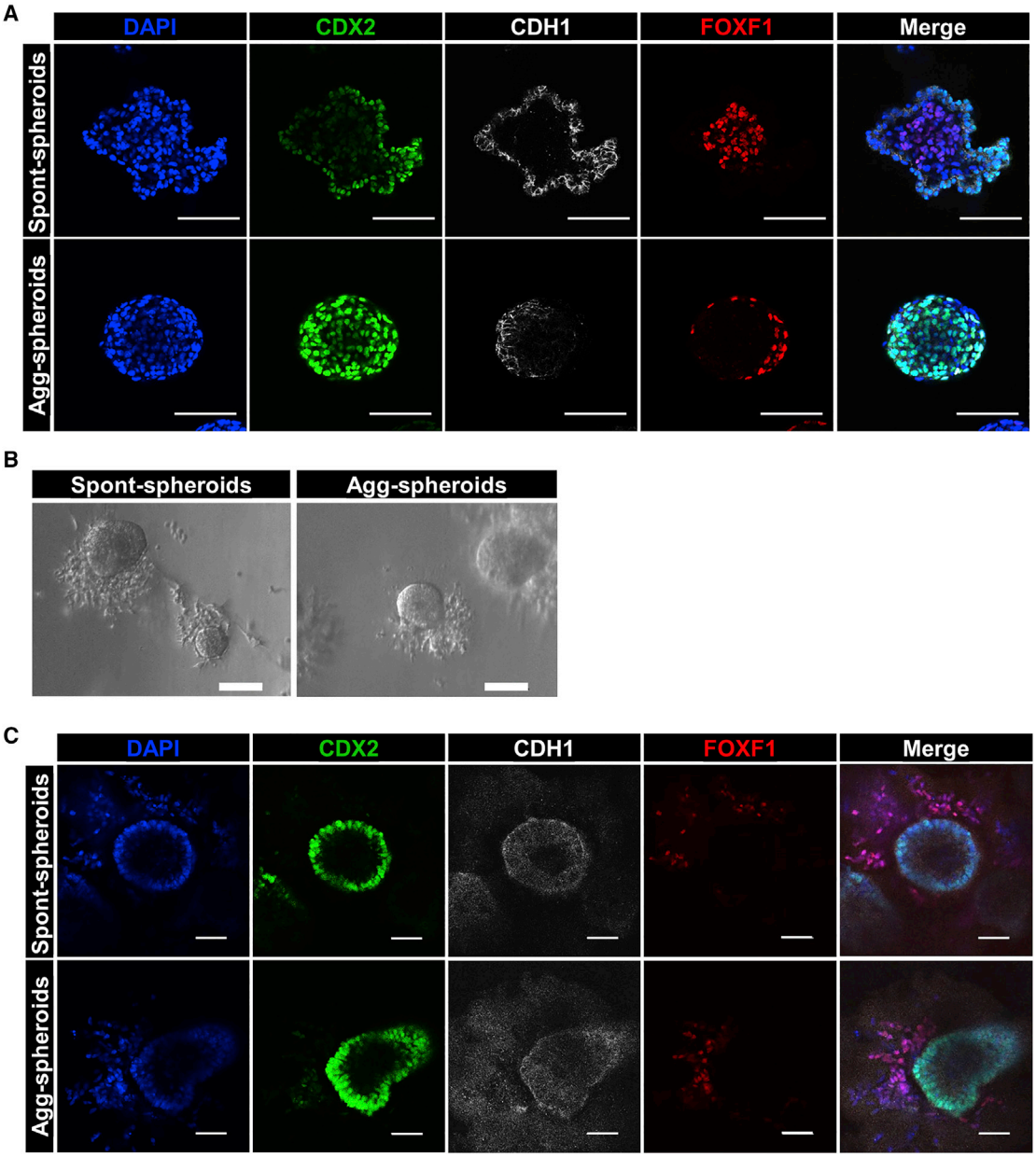

Figure 4. Agg-spheroids maintain intestinal marker expression and mesenchyme expansion

(A) H1-derived day 7 spont-spheroids and day 8 agg-spheroids were harvested, fixed, and subjected to whole-mount immunostaining for intestinal epithelial (CDX2 and CDH1) and mesenchymal (FOXF1) markers. Scale bar, 100 μm.

(B) Representative images of the gross morphology of H1-derived spont- and agg-spheroids 3 days after embedding in Matrigel. Scale bar, 100 μm.

(C) H1-derived spont- and agg-spheroids were fixed after 3 days of culture in Matrigel and subjected to whole-mount immunostaining to identify intestinal epithelia (CDH1/CDX2) and mesenchymal (FOXF1) cells. Scale bar, 100 μm.

into the mesentery or kidney capsule of immunodeficient NSG mice. Of 9 agg-HIOs transplanted into the mesentery, 8 resulted in engraftment and organoid growth, while all 5 agg-HIOs transplanted under the kidney capsule resulted in engraftment. After harvesting engrafted organoids, H&E-stained sections were prepared and intestinal histology and lumen maturity grade analyzed (Singh et al., 2020). Transplanted agg-HIOs contained multiple lumens (mesentery: 4.2 ± 2.1; kidney: 2.6 ± 0.5) and stereotypical formation of mature small intestine-like crypt-villus structures

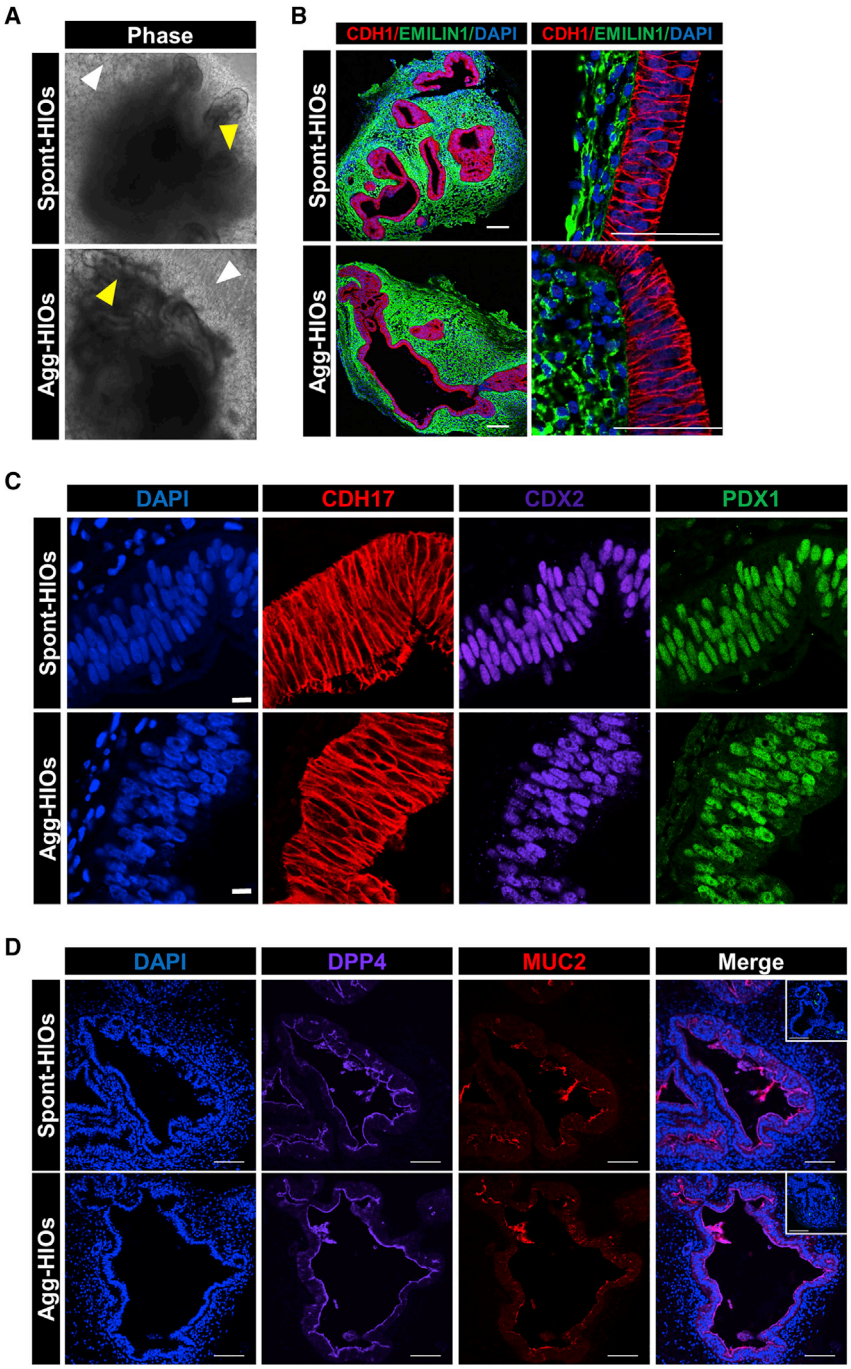

Figure 5. Growth and cytodifferentiation of agg-HIOs is similar to spont-HIOs

(A) Gross morphology of organoids produced from H1-derived spont-spheroids (spont-HIOs) and agg-spheroids (agg-HIOs) is similar on day 35. Organoids consisted of convoluted epithelial layers (yellow arrow) surrounded by an outgrowth of mesenchymal cells (white arrow).

(B) Sections of day 35 HIOs were immunostained with antibodies to CDH1 (epithelia) and Emilin1 (mesenchyme) and counterstained with DAPI. Scale bars, 100 μm.

(C) Sections from day 35 HIOs were immunostained with antibodies to CDH17, CDX2, and PDX1. Sections were counterstained with DAPI. Scale bars, 10 μm.

(D) Sections from day 35 HIOs were immunostained with antibodies to DPP4, MUC2, and CHGA (inset, green). Immunofluorescence staining of day 35 spont- and agg-HIOs. Scale bar, 100 μm.

(Figures S5A and S5B). The maturity grade of agg-HIOs engrafted in the mesentery was 2.4 ± 0.8, while kidney capsule-engrafted agg-HIOs were more mature, with a grade of 3.3 ± 0.3. These scores are within the reported range for transplanted spont-HIOs (Singh et al., 2020) and demonstrate that agg-HIOs retain the capacity to undergo further growth and maturation *in vivo*. Finally, the detection of sucrose isomaltase (SI; enterocytes), MUC2 (goblet cells) and CHGA (enteroendocrine cells) confirmed the presence of both absorptive and secretory lineages in the epithelia of transplanted agg-HIOs (Figure S5C).

Together, these data demonstrate that the *in vitro* growth and cytodifferentiation of agg-HIOs and the ability to differentiate to mature intestinal-like tissue *in vivo* is similar to spont-HIOs, confirming that MHE aggregation represents a robust method for the reproducible generation of HIOs.

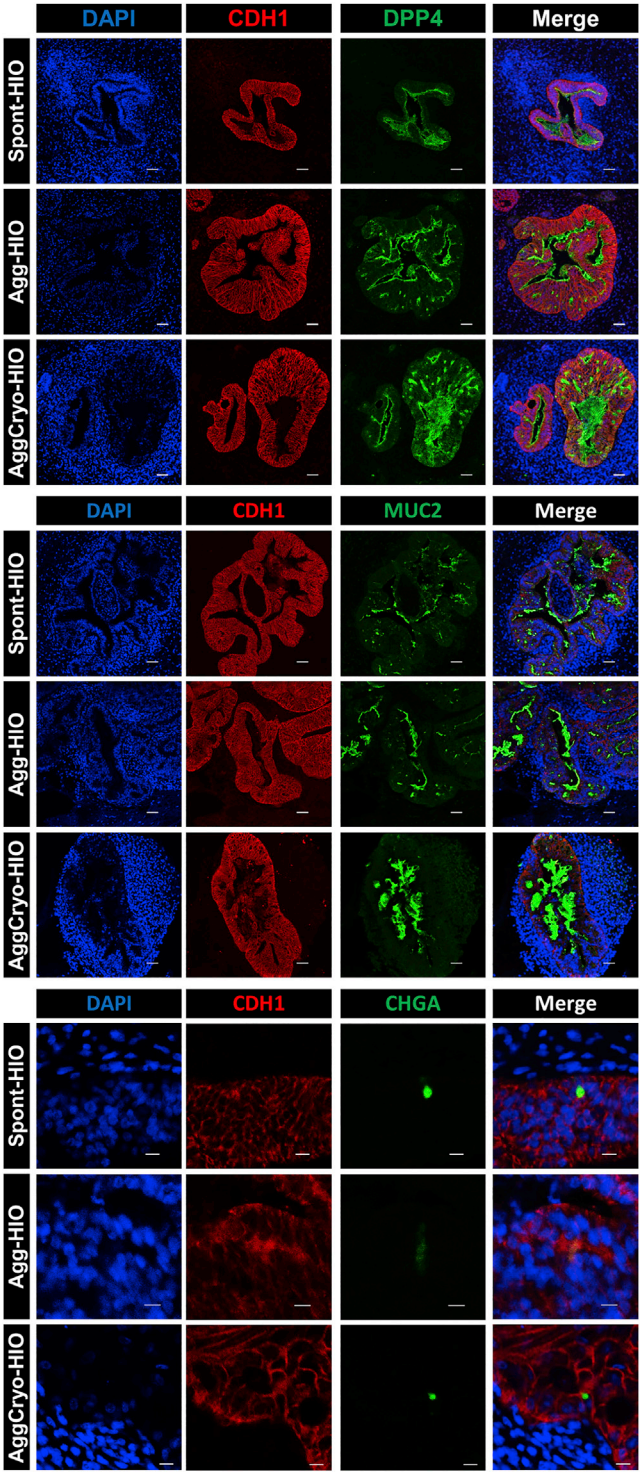

Figure 6. Generation of HIOs from cryopreserved agg-spheroids

H1-derived spont-, agg-, and cryoagg-HIOs demonstrate similar expression of HIO differentiation markers DPP4, MUC2, and CHGA. Sections of day 35 spont-, agg-, and cryoagg HIOs were immunostained with antibodies to CDH1, DPP4, MUC2, and CHGA and counterstained with DAPI. Top and center panels scale bars, 100 μM. Bottom panel scale bar, 20 μm.

MHE cryopreservation for HIO generation

Effective implementation of protocols for HIO generation is challenging and requires significant technical expertise and time, including the daily maintenance of hPSC cultures and differentiation to DE and MHE. This has limited the widespread adoption of hPSC-derived HIO technologies. We reasoned that one solution would be to cryopreserve, thaw, and aggregate MHE progenitors for HIO production. Therefore, we dissociated MHE monolayers to single cells before cryopreservation and storage in liquid nitrogen (liN2). Upon thawing and aggregation of MHE, spheroids were formed (cryoagg-spheroids; data not shown) that generated organoids after Matrigel embedding. Interestingly, in contrast to control spont- and agg-HIOs, culture of cryoagg-spheroids in standard HIO media was associated with significant mispatterning, generating organoids containing very few $CDH17^{+}/CDX2^{+}$ small intestinal epithelial cells (Figure S6A). However, epithelial mispatterning was completely reversed when cryoagg-spheroids were cultured in HIO media without NOGGIN (Figure S6A). We therefore removed NOGGIN from HIO media for all of the subsequent experiments using cryopreserved MHE. The size and morphology of organoids derived from thawed MHE was comparable to aggregated MHE that had not been cryopreserved (Figures S6B and S6C), and automated analysis of the lumen area in randomly selected organoid sections from 3 hPSC lines demonstrated no significant difference between agg-HIOs and cryoAgg-HIOs (Figure S6D). Finally, immunofluorescence analysis of the expression of markers of intestinal epithelial differentiation demonstrated similar expression of DPP4, MUC2, and CHGA in spont-, agg-, and cryoagg-HIOs (Figure 6). Together, these data demonstrate that MHE can be cryopreserved, thawed, and aggregated without compromising the ability to form HIOs containing differentiated small intestinal epithelial cells. However, culture in the absence of NOGGIN is essential to generate appropriately patterned HIOs.

Production of antral stomach and colonic organoids by aggregation

We next determined whether aggregation was applicable to other hPSC-derived GI organoid protocols, specifically colonic organoids (HCO) (Munera et al., 2017) and antral stomach organoids (HAGO) (McCracken et al., 2014). For HCO generation, spont- and agg-spheroids from MHE were embedded in Matrigel, exposed to bone morphogenetic protein-2 (BMP2) for 3 days and cultured until day 35. Developing HCOs derived from spont- and agg-spheroids were

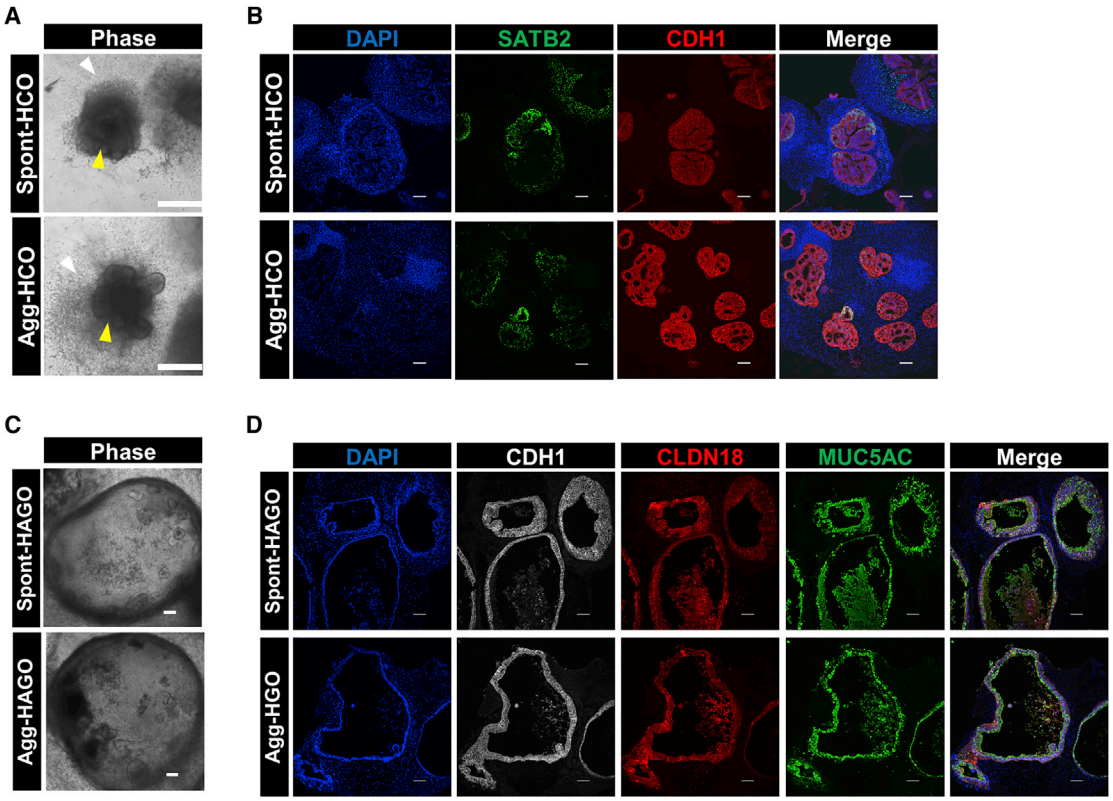

Figure 7. Generation of colonic and antral gastric organoids by aggregation

(A) Gross morphology of colonic organoids derived from BMP2 patterned spont- and agg-spheroids at day 33 showing epithelial (yellow arrow) and mesenchymal (white arrow) cell layers. Scale bars, 500 μm.

(B) Sections of spont- and agg-HCO harvested at day 35 were prepared and co-immunostained for hindgut epithelial cell markers SATB2 and CDH1. Sections were counterstained with DAPI to label nuclei. Scale bars, 100 μm.

(C) Representative images of organoids at day 32 of culture are shown. Scale bar, 100 μm.

(D) Sections of day 32 spont- and agg-HAGOs were co-immunostained for antral stomach epithelial cell markers Claudin 18 (CLDN18), Mucin 5AC (MUC5AC), and E-cadherin (CDH1). Nuclei were counterstained with DAPI. Scale bars, 100 μm.

morphologically similar, exhibiting convoluted epithelial layers surrounded by an outgrowth of mesenchymal cells (Figure 7A). Immunofluorescence analysis of day 35 organoids derived from spont- and agg-spheroids demonstrated the formation of a CDX2$^+$ epithelia surrounded by EMILIN1$^+$ mesenchyme (Figure S7A) that was positive for the colon-specific marker SATB2 (Munera et al., 2017) and contained abundant MUC2$^+$ goblet cells (Figures 7B and S7B). qRT-PCR analysis of colon-enriched markers SATB2, HOXA13, and HOXD13 demonstrated no significant difference in the expression of these genes between spont- and agg-HCOs. However, expression of these genes was significantly higher in HCOs than in HAGOs (Figure S7G).

We next investigated whether aggregation could generate foregut-derived HAGOs. After posterior foregut endoderm (PFE) specification, a uniform SOX2$^+$/CDX2$^-$ monolayer and free-floating spont-spheroids were generated (Figure S7C). Spont-spheroids were collected and embedded in Matrigel. The remaining PFE monolayer was then subjected to overnight aggregation in Aggrewell 400 plates before embedding in Matrigel (agg-spheroids). PFE monolayers robustly and reproducibly generated consistent aggregates in microwells (Figure S7D). PFE-derived spont- and agg-spheroids were then cultured until day 35 to generate spont-HAGOs and agg-HAGOs, respectively. There was no discernible morphological difference between spont-HAGOs and agg-HAGOs at any stage of their formation (Figure 7C). Immunofluorescence analysis demonstrated that both spont-HAGOs and agg-HAGOs contained SOX2$^+$/PDX1$^+$/GATA4$^+$ posterior foregut (Figures S7E and S7F) and expressed antral specific markers CLDN18 and MUC5AC (Figure 7D). qRT-PCR analysis demonstrated that the expression of antrum-enriched markers CLDN18, MUC5AC, and PDX1 was not significantly different between spont- and agg-HAGOs but significantly higher than in HCOs (Figure S7G). Finally, levels of CDH17 and

MUC2, enriched in intestine, were significantly lower in spont- and agg-HAGOs than in HIOs (Figure S7G).

Together, these data demonstrate that an aggregation-based approach is broadly applicable to the generation of PSC-derived GI organoids.

DISCUSSION

The major challenge in the successful development of HIOs from hPSCs is the requirement for spontaneous morphogenesis to produce free-floating MHE spheroids. Spontaneous morphogenesis is independent of qualitative differences in hPSC seeding density and is associated with significant variability in spheroid production and/or detachment. Non-detached spheroids can be manually excised and embedded, but this is labor intensive and not amenable to scale up for translational applications. Variability is manifested between hPSC cell lines, as well as from experiment to experiment, and even from well to well. Here, we describe a robust solution that eliminates this variability to facilitate reliable and reproducible HIO generation via the aggregation of MHE monolayers. We consistently generated 10- to 20-fold higher spheroid yield than could be achieved through spontaneous morphogenesis. Furthermore, MHE monolayers can be dissociated, cryopreserved, and subsequently thawed and aggregated to produce HIOs. Finally, we also demonstrate that aggregation is effective for generating human antral stomach and colonic organoids from hPSCs.

Essential to the full dissemination of this technology is the ability to cryopreserve organoids. To our knowledge, no reliable method is currently available to cryopreserve and successfully thaw fully functional hPSC-derived HIOs. Here, we show that HIOs can be produced by the aggregation of cryopreserved MHE monolayers. Interestingly, while agg-spheroids generated from non-cryopreserved MHE are robustly patterned to CDH17$^+$ small intestine in HIO media containing NOGGIN, cryopreserved MHE required the removal of NOGGIN from HIO media to generate properly patterned small intestinal organoids. This suggests that cryo-agg-spheroids are more sensitive to reductions in endogenous BMP signaling than agg-spheroids. Regardless, this slight modification to the protocol permits the preparation and long-term storage of quality-controlled banks of cryopreserved MHE, enabling the distribution of cells that can be directly aggregated and used for HIO production. Furthermore, the ability to distribute cryopreserved batches of MHE for aggregation greatly simplifies the process of HIO production and facilitates access to HIO technologies for any lab without the need for technical staff to have expertise in hPSC culture and differentiation.

In addition to the production of small intestinal organoids, our data demonstrates that aggregation can be used to reliably produce human stomach and colon organoids. These findings suggest that our approach may be broadly applicable to the production of organoids from additional GI tissues in which spontaneous detachment of spheroids is required (e.g., esophageal [Trisno et al., 2018] or fundic stomach [McCracken et al., 2017] organoids). This idea is being currently tested. While we show that cryopreserved and thawed MHE cells can be aggregated to produce HIOs, it will be important to investigate the impact of cryopreservation, thawing, and aggregation on the production of other endoderm-derived organoid types. Given that successful cryopreservation of PFE and thawing for liver organoid production has been previously described (Shinozawa et al., 2021), we anticipate that cryopreserved/thawed PFE will also be suitable for aggregation to produce antral and fundic gastric organoids.

In summary, we describe an improved method for the reproducible, scalable production of hPSC-derived small intestinal organoids that overcomes the unreliable spontaneous production of detached MHE spheroids to facilitate robust HIO production from all hPSC lines tested, regardless of the quantity of spontaneous morphogenesis. We demonstrate that with a minor modification to the protocol, MHE can be cryopreserved, thawed, and aggregated to produce HIOs, providing a simple method for the large-scale production of quality-controlled frozen banks of MHE from high-priority hPSC lines that will provide a consistent source of cells for subsequent HIO production without the need to continuously culture hPSCs. Distribution of cells from these banks will also greatly enhance and facilitate successful dissemination of HIO technologies by eliminating the need for receiving laboratories to be trained in hPSC culture and differentiation to DE and MHE. Furthermore, in combination with approaches that facilitate HIO production from spheroids in suspension culture (Capeling et al., 2022), generation of MHE spheroids by aggregation may significantly enhance translational efforts by both increasing scalability and reducing hands-on labor requirements. Finally, we show that aggregation can be applied to the production of colonic and antral stomach organoids, indicating that additional GI organoid types can be reliably produced by this method. Ultimately, we envision that this method will facilitate "plug-and-play" access to scalable human GI organoid generation that will enhance dissemination and significantly increase access to these technologies.

EXPERIMENTAL PROCEDURES

Human hESC and iPSC culture

Human pluripotent stem cells were cultured under feeder-free conditions using mTeSR1 (StemCell Technologies) and hESC-qualified Matrigel (Corning 354277) and incubated at 37°C with 5% CO_2 in

air. Cells were passaged weekly using Gentle Cell Dissociation Reagent (StemCell Technologies).

Generation of human iPSCs

Human ESC line (WA01) was obtained from WiCell. Human iPSCs used in this study were generated in the Cincinnati Children's Hospital Medical Center Pluripotent Stem Cell Facility. Generation of iPSC72_3 has been described previously (McCracken et al., 2014). iPSC75_1 and iPSC115_1 were also generated by this same procedure, using fibroblasts cultured from discarded circumcision tissue obtained from 2 healthy donors (provided by Dr. Susanne Wells, Division of Hematology/Oncology, Cincinnati Children's Hospital Medical Center [CCHMC]; institutional review board no. 02-9-29X). Line iPSC285_1 was derived from a skin biopsy obtained from a healthy female donor (provided by Dr. Vivian Hwa, Division of Endocrinology, CCHMC; institutional review board no. 2014–5919), and generated using the same procedure. All of the experiments with human PSCs were approved by the Cincinnati Children's Hospital ESCRO committee (protocol no. EIPDB108).

Differentiation into human intestinal organoids

Differentiation of hPSC lines into HIOs was performed as previously described (McCracken et al., 2011; Spence et al., 2011), with minor modifications. Briefly, hPSC clusters were exposed to DE media consisting of RPMI 1640 containing 1× non-essential amino acids, containing 100 ng/mL activin A containing 0%, 0.2%, and 2% defined fetal calf serum (FCS) on days 1, 2, and 3, respectively. In some experiments, hPSCs were plated as single cells at 1.5×10^5 cells/well after accutase dissociation in mTeSR1 containing 10 μM Y27632. Starting on day 4, cells were fed daily for 4 days with MHE media consisting of RPMI 1640 media containing 1× non-essential amino acids, containing 2% defined FCS, human recombinant FGF4 (500 ng/mL; Shenandoah Biotechnology), and CHIR99021 (3 μM; StemCell Technologies) to generate mid-/hindgut endoderm. On day 7, detached spheroids were embedded in Matrigel as previously described (McCracken et al., 2011). Briefly, spheroids were collected and ∼250 embedded into 50 μL ice-cold Matrigel (Corning 354234), which was plated into the center of a single well of a 24-well plate. The plate was then inverted and incubated at 37°C for 10 min to polymerize Matrigel. HIO media, consisting of Advanced DMEM/F12, 1× B27 supplement + insulin, 1× N2 supplement, 15 mM HEPES buffer, 1× penicillin/streptomycin, 1× L-glutamine containing NOGGIN (100 ng/mL), epidermal growth factor (100 ng/mL), and 5% R-SPONDIN conditioned media (Sato et al., 2011) was replaced every 2–3 days. For the generation of HIOs from cryopreserved MHE, HIO media lacking NOGGIN was used. HIOs were manually passaged to reduce tissue density on approximately day 21 (McCracken et al., 2011) and harvested on day 35.

Cryopreservation and aggregation of mid-/hindgut monolayers

To produce aggregated MHE spheroids from day 7 MHE monolayers, hPSCs were sequentially exposed to DE media and MHE media as described above. MHE monolayers were incubated with accutase to generate a single-cell suspension (detached spheroids were not collected). Cells were washed in RPMI 1640 and pelleted by centrifugation. For cryopreservation, the MHE cell pellet was resuspended at 3.6×10^6 cells/mL in ice-cold CellBanker1 (AMSBIO), frozen overnight in a Mr. Frosty, and transferred to liN2 for long-term storage. Vials containing frozen MHE were thawed rapidly and cells were washed in cold Advanced DMEM/F12. For aggregation, freshly generated or thawed MHE was resuspended in HIO media-NOGGIN + 10 μM Y-27632, and the cell number was determined. Aggrewell 400 plates containing 1,200 microwells per well (StemCell Technologies) were prepared using Aggrewell rinsing solution following the manufacturer's instructions. For aggregation, 3.6×10^6 MHE cells per well, corresponding to 3,000 cells per microwell, were added to the Aggrewell 400 plate in HIO media containing 10 μM Y-27632 and mixed by pipetting to ensure even distribution. The plate was then centrifuged at 100 x *g* for 3 min to pellet the cells in microwells and incubated overnight. The next day, aggregated MHE spheroids were collected and ∼250 were embedded in 50 μL ice-cold Matrigel (Corning 354237). Matrigel droplets were then plated in a single well of a 24-well dish as described (McCracken et al., 2011), except when cryopreserved MHE was aggregated, where HIO media lacking NOGGIN was used. In most experiments, MHE agg-spheroids generated from aggregated monolayers were directly compared to spont-spheroids derived in the same experiment.

Generation of aggregated colonic and antral stomach organoids

For colonic organoid formation, spont- and agg-spheroids was generated from MHE as described above. After embedding in Matrigel, spheroids were exposed to 100 ng/mL BMP2 (R&D Systems) for 3 days to posteriorize MHE and cultured for HCO generation as previously described (Munera et al., 2017). For antral stomach organoid production, PFE was generated as previously described (McCracken et al., 2014). On day 6 of PFE differentiation, spont-spheroids were collected, and agg-spheroids were generated by aggregating 3.6×10^6 PFE cells per well of an Aggrewell 400 plate. After embedding in Matrigel, spont- and agg-PFE spheroids were cultured for antral organoid generation exactly as described (Broda et al., 2019).

Organoid processing for sectioning and staining

Spheroids and organoids were harvested in ice-cold dPBS, pipetted to remove Matrigel, rinsed with dPBS, fixed with 4% paraformaldehyde at 4°C for 1 h with rotation, and washed with cold dPBS for 3 × 30 min at 4°C with rotation. After fixation, organoids were used for whole-mount immunostaining or subject to routine paraffin embedding and sectioning at 7 μm. After deparaffinizing and rehydrating, slides were used immediately for histological staining or exposed to heat-induced epitope retrieval for immunostaining and subsequent analysis.

Immunofluorescence analysis

Cells were fixed with 4% paraformaldehyde in dPBS for 15 min at room temperature, washed 3 × 5 min with dPBS, permeabilized in dPBS containing 0.5% Triton X-100 for 15 min, and blocked using blocking buffer consisting of dPBS containing 0.5% Triton X-100 and 5% normal donkey serum (Jackson Laboratories) for 30 min.

Slides were deparaffinized, subject to antigen retrieval, and washed and blocked for 30 min at room temperature. Cells and sections were incubated in primary antibodies (see Table S1) diluted in blocking buffer at 4°C overnight, washed 3 × 5 min in dPBS, and incubated with appropriate fluorescent-conjugated secondary antibodies for 1 h at room temperature. After washing (3 × 5 min with dPBS) cells and sections were counterstained with DAPI and subjected to imaging. Whole-mount immunostaining of spheroids was performed as previously described (Munera et al., 2017). See Table S1 for a list of antibodies used in this study and dilutions. Confocal images of immunostained sections and whole mounts were captured on a Nikon A1 confocal wide-field microscope. Images of immunostained monolayers were captured on Nikon Ti-E SpectraX inverted wide-field microscope.

Short tandem repeat (STR) profiling

To authenticate the identity of each cell line used in this study, STR profiling was conducted by LabCorp. The markers analyzed were D3S1358, TH01, D21S11, D18S51, Penta E, D5S818, D13S317, D7S820, D16S539, CSF1PO, Penta D, vWA, D8S1179, TPOX, FGA, and AMEL. The STR profile obtained from H1 (WA01) cells matched the profile for all tested loci reported for this line on Cellosaurus (https://web.expasy.org/cellosaurus/CVCL_9771). The STR profile of each iPSC line used in this study matched all of the tested loci of the respective donor cells.

Flow cytometry for stemness markers

hPSCs were harvested by Accutase dissociation at 37°C for ~5 min, centrifuged for 3 min at 300 x *g*, and washed with ice-cold fluorescence-activated cell sorting (FACS) buffer consisting of dPBS containing 0.2% w/v bovine serum albumin (BSA) and 0.05% sodium azide. To remove cell clumps, cells were passed through a 40-μm cell strainer and 1×10^6 cells were co-labeled with AlexaFluor 647-conjugated mouse anti-human SSEA4 antibody (diluted 1:40) and fluorescein isothiocyanate (FITC)-conjugated mouse anti-human Tra-1-60 antibody (diluted 1:20) for 30 min on ice. Cell viability was determined by staining with 7-AAD (eBioscience). After labeling, cells were washed with FACS buffer and resuspended in 100 μL ice-cold FACS buffer. Flow cytometry was performed on a Canto flow cytometer, and data were analyzed using FACSDIVA software.

Calculation of spont- and agg-spheroid area

Spont- and agg-spheroids were harvested and placed into one side of a 2-chamber cell culture slide (Thermo Fisher Scientific). Spheroids were allowed to settle to the bottom of the chamber before imaging the entire surface of each chamber with a Keyence BZ-X710 imaging system. Each image was then analyzed using Keyence BZ-X800 Analyzer software to count the total number of spheroids in the chamber and define the perimeter of each spheroid not touching the edge of each image. The perimeter was then used to calculate the area of each spheroid. Images were also stitched to produce an image of the whole chamber. In some experiments, images were imported into ImageJ, distance calibrated using the image scale bar, and the diameter of each spheroid calculated by manually drawing a line across each spheroid.

hPSC scorecard data analysis

Functional pluripotency of each hPSC line used in this study was assessed using the Applied Biosystems TaqMan hPSC Scorecard Panel (Thermo Fisher Scientific). Total RNA from undifferentiated hPSCs and EBs differentiated for 14 days was isolated using the Qiagen RNeasy Plus Mini Kit (Qiagen), and 1 μg RNA was reverse transcribed to cDNA using the Super-Script VILO cDNA Synthesis Kit (Thermo Fisher Scientific). TaqMan qRT-PCR was carried out using the hPSC Scorecard 384w Fast Plate (Thermo Fisher Scientific, A15870) on a QuantStudio 7 qPCR device following the manufacturer's recommended protocol. Gene expression data from the Scorecard Panel were analyzed using the web-based hPSC Scorecard Analysis Software (Thermo Fisher Scientific).

TaqMan and qRT-PCR analysis

Day 35 organoids were collected in RA1 Lysis Buffer with β-mercapethanol and stored at −80°C until all of the samples were collected. Total RNA was isolated using NucleoSpin RNA Isolation Kit (Macherey-Nagel) according to the manufacturer's instructions. cDNA was generated using the Super-Script VILO cDNA Synthesis Kit (Invitrogen). qRT-PCR was performed using PowerUp SYBR Green Master Mix (Applied Biosystems) and detected on a QuantStudio 3 Real-Time PCR thermocycler (Applied Biosystems). Primer sequences are available upon request. Analysis was performed using the ΔΔCt method and normalized to the housekeeping gene PPIA. TaqMan (Applied Biosystems) gene expression assays were performed in a One-Step thermocycler (Applied Biosystems) using β-actin as a reference gene (see Table S2).

Mesentery and renal subcapsular HIO transplantation

All of the animal work was performed with the prior approval of CCHMC's Institutional Animal Care and Use Committee (protocol no. 2018-0092). Mice were housed in the pathogen-free animal vivarium of CCHMC. Handling was performed humanely in accordance with the NIH *Guide for the Care and Use of Laboratory Animals*. Transplantation experiments used male and female non-obese diabetic (NOD) severe combined immunodeficiency (SCID) interleukin 2-Rγ null (NSG) mice between 50 and 70 days of age. A single D35 agg-HIO was transplanted in either the mouse mesentery or renal subcapsular space, as previously described (Singh et al., 2020). After 8–12 weeks, mice were euthanized and engrafted organoids were harvested, fixed, paraffin embedded, and sectioned for routine H&E staining and immunostaining. Lumen grades of transplanted agg-HIOs were determined as described (Singh et al., 2020).

Statistics

Data are presented as the mean ± SD or the mean ± SEM Non-parametric comparisons for 2 groups were calculated by Mann-Whitney *U* test. Unless indicated otherwise, comparisons for more than 2 groups were calculated by ANOVA followed by the Kruskal-Wallis test and the Dunn multiple comparison test for data with non-normal distribution with $p < 0.05$ considered significant.

SUPPLEMENTAL INFORMATION

Supplemental information can be found online at https://doi.org/10.1016/j.stemcr.2022.06.011.

AUTHOR CONTRIBUTIONS

Conceptualization, C.N.M., A.L.P., and P.L.L.; methodology, C.N.M., A.L.P., and P.L.L.; investigation, A.L.P., H.M.P., M.A.S., N.S., P.L.L., J.G.S., D.O.K., and T.R.B.; formal analysis, C.N.M., A.L.P., H.M.P., D.O.K., and P.L.L.; resources, C.N.M., M.A.H., and J.M.W.; writing – original draft, C.N.M.; writing – review & editing, C.N.M., A.L.P., H.M.P., and J.M.W.; supervision, C.N.M.

ACKNOWLEDGMENTS

The authors would like to thank members of the Zorn and Wells labs for insightful comments about this work, and Dr. Wendy L Thompson for assistance with the Keyence system and critical review of the manuscript; Dr. Andrew Dunn for assistance with Keyence BZ-X800 Analyzer software; and Dr. Magdalena Kasendra for critical review of the manuscript. We also acknowledge the Research Flow Cytometry Core, Veterinary Services Core, and Pathology Research Core for their assistance with this study. This project was supported in part by NIH P30 DK078392 (Stem Cell Organoid and Genome Editing Core of the Digestive Diseases Research Core Center in Cincinnati). This research was also supported by grants from the NIH (U18 EB021780, to J.M.W. and M.A.H.; U19 AI116491, P01 HD093363, and UG3 DK119982, to J.M.W.; U01 DK103117, to M.A.H.; the Shipley Foundation, to J.M.W., the Paul G. Allen Family Foundation, to J.M.W.; and the Pursuing Our Potential Together effort of Cincinnati Children's Hospital.

CONFLICTS OF INTEREST

The authors declare no competing interests.

Received: September 9, 2021
Revised: June 29, 2022
Accepted: June 30, 2022
Published: July 28, 2022

REFERENCES

Broda, T.R., McCracken, K.W., and Wells, J.M. (2019). Generation of human antral and fundic gastric organoids from pluripotent stem cells. Nat. Protoc. *14*, 28–50. https://doi.org/10.1038/s41596-018-0080-z.

Capeling, M.M., Huang, S., Childs, C.J., Wu, J.H., Tsai, Y.H., Wu, A., Garg, N., Holloway, E.M., Sundaram, N., Bouffi, C., et al. (2022). Suspension culture promotes serosal mesothelial development in human intestinal organoids. Cell Rep. *38*, 110379. https://doi.org/10.1016/j.celrep.2022.110379.

Chambers, S.M., Fasano, C.A., Papapetrou, E.P., Tomishima, M., Sadelain, M., and Studer, L. (2009). Highly efficient neural conversion of human ES and iPS cells by dual inhibition of SMAD signaling. Nat. Biotechnol. *27*, 275–280. https://doi.org/10.1038/nbt.1529.

Cortez, A.R., Poling, H.M., Brown, N.E., Singh, A., Mahe, M.M., and Helmrath, M.A. (2018). Transplantation of human intestinal organoids into the mouse mesentery: a more physiologic and anatomic engraftment site. Surgery *164*, 643–650. https://doi.org/10.1016/j.surg.2018.04.048.

Du, A., McCracken, K.W., Walp, E.R., Terry, N.A., Klein, T.J., Han, A., Wells, J.M., and May, C.L. (2012). Arx is required for normal enteroendocrine cell development in mice and humans. Dev. Biol. *365*, 175–188. https://doi.org/10.1016/j.ydbio.2012.02.024.

Forbester, J.L., Goulding, D., Vallier, L., Hannan, N., Hale, C., Pickard, D., Mukhopadhyay, S., and Dougan, G. (2015). Interaction of Salmonella enterica serovar typhimurium with intestinal organoids derived from human induced pluripotent stem cells. Infect. Immun. *83*, 2926–2934. https://doi.org/10.1128/IAI.00161-15.

Hannan, N.R.F., Fordham, R.P., Syed, Y.A., Moignard, V., Berry, A., Bautista, R., Hanley, N.A., Jensen, K.B., and Vallier, L. (2013). Generation of multipotent foregut stem cells from human pluripotent stem cells. Stem Cell Rep. *1*, 293–306. https://doi.org/10.1016/j.stemcr.2013.09.003.

Kim, J., Koo, B.K., and Knoblich, J.A. (2020). Human organoids: model systems for human biology and medicine. Nat. Rev. Mol. Cell. Biol. *21*, 571–584. https://doi.org/10.1038/s41580-020-0259-3.

Kokkinaki, M., Sahibzada, N., and Golestaneh, N. (2011). Human induced pluripotent stem-derived retinal pigment epithelium (RPE) cells exhibit ion transport, membrane potential, polarized vascular endothelial growth factor secretion, and gene expression pattern similar to native RPE. Stem. Cell. *29*, 825–835. https://doi.org/10.1002/stem.635.

Kumar, S.V., Er, P.X., Lawlor, K.T., Motazedian, A., Scurr, M., Ghobrial, I., Combes, A.N., Zappia, L., Oshlack, A., Stanley, E.G., and Little, M.H. (2019). Kidney micro-organoids in suspension culture as a scalable source of human pluripotent stem cell-derived kidney cells. Development *146*, dev172361. https://doi.org/10.1242/dev.172361.

Leslie, J.L., Huang, S., Opp, J.S., Nagy, M.S., Kobayashi, M., Young, V.B., and Spence, J.R. (2015). Persistence and toxin production by Clostridium difficile within human intestinal organoids result in disruption of epithelial paracellular barrier function. Infect. Immun. *83*, 138–145. https://doi.org/10.1128/iai.02561-14.

McCauley, H.A., Matthis, A.L., Enriquez, J.R., Nichol, J.T., Sanchez, J.G., Stone, W.J., Sundaram, N., Helmrath, M.A., Montrose, M.H., Aihara, E., and Wells, J.M. (2020). Enteroendocrine cells couple nutrient sensing to nutrient absorption by regulating ion transport. Nat. Commun. *11*, 4791. https://doi.org/10.1038/s41467-020-18536-z.

McCracken, K.W., Aihara, E., Martin, B., Crawford, C.M., Broda, T., Treguier, J., Zhang, X., Shannon, J.M., Montrose, M.H., and Wells, J.M. (2017). Wnt/beta-catenin promotes gastric fundus specification in mice and humans. Nature *541*, 182–187. https://doi.org/10.1038/nature21021.

McCracken, K.W., Catá, E.M., Crawford, C.M., Sinagoga, K.L., Schumacher, M., Rockich, B.E., Tsai, Y.H., Mayhew, C.N., Spence, J.R., Zavros, Y., and Wells, J.M. (2014). Modelling human development and disease in pluripotent stem-cell-derived gastric organoids. Nature *516*, 400–404. https://doi.org/10.1038/nature13863.

McCracken, K.W., Howell, J.C., Wells, J.M., and Spence, J.R. (2011). Generating human intestinal tissue from pluripotent stem cells in vitro. Nat. Protoc. *6*, 1920–1928. https://doi.org/10.1038/nprot.2011.410.

Merkert, S., Schubert, M., Olmer, R., Engels, L., Radetzki, S., Veltman, M., Scholte, B.J., Zöllner, J., Pedemonte, N., Galietta, L.J.V., and Martin, U. (2019). High-Throughput screening for modulators of CFTR activity based on genetically engineered cystic fibrosis disease-specific iPSCs. Stem Cell Rep. *12*, 1389–1403. https://doi.org/10.1016/j.stemcr.2019.04.014.

Múnera, J.O., Sundaram, N., Rankin, S.A., Hill, D., Watson, C., Mahe, M., Vallance, J.E., Shroyer, N.F., Sinagoga, K.L., Zarzoso-Lacoste, A., and Wells, J.M. (2017). Differentiation of human pluripotent stem cells into colonic organoids via transient activation of BMP signaling. Cell Stem Cell *21*, 51–64.e6. https://doi.org/10.1016/j.stem.2017.05.020.

Onozato, D., Ogawa, I., Kida, Y., Mizuno, S., Hashita, T., Iwao, T., and Matsunaga, T. (2021). Generation of budding-like intestinal organoids from human induced pluripotent stem cells. J. Pharm. Sci. *110*, 2637–2650. https://doi.org/10.1016/j.xphs.2021.03.014.

Onozato, D., Yamashita, M., Nakanishi, A., Akagawa, T., Kida, Y., Ogawa, I., Hashita, T., Iwao, T., and Matsunaga, T. (2018). Generation of intestinal organoids suitable for pharmacokinetic studies from human induced pluripotent stem cells. Drug. Metab. Dispos. *46*, 1572–1580. https://doi.org/10.1124/dmd.118.080374.

Ortmann, D., and Vallier, L. (2017). Variability of human pluripotent stem cell lines. Curr. Opin. Genet. Dev. *46*, 179–185. https://doi.org/10.1016/j.gde.2017.07.004.

Sato, T., Van Es, J.H., Snippert, H.J., Stange, D.E., Vries, R.G., Van Den Born, M., Barker, N., Shroyer, N.F., van de Wetering, M., and Clevers, H. (2011). Paneth cells constitute the niche for Lgr5 stem cells in intestinal crypts. Nature *469*, 415–418. https://doi.org/10.1038/nature09637.

Shinozawa, T., Kimura, M., Cai, Y., Saiki, N., Yoneyama, Y., Ouchi, R., Koike, H., Maezawa, M., Zhang, R.R., Dunn, A., et al. (2021). High-fidelity drug-induced liver injury screen using human pluripotent stem cell-derived organoids. Gastroenterology *160*, 831–846.e10. https://doi.org/10.1053/j.gastro.2020.10.002.

Singh, A., Poling, H.M., Sundaram, N., Brown, N., Wells, J.M., and Helmrath, M.A. (2020). Evaluation of transplantation sites for human intestinal organoids. PLoS One *15*, e0237885. https://doi.org/10.1371/journal.pone.0237885.

Sommer, C.A., Capilla, A., Molina-Estevez, F.J., Gianotti-Sommer, A., Skvir, N., Caballero, I., Chowdhury, S., and Mostoslavsky, G. (2018). Modeling APC mutagenesis and familial adenomatous polyposis using human iPS cells. PLoS One *13*, e0200657. https://doi.org/10.1371/journal.pone.0200657.

Son, Y.S., Ki, S.J., Thanavel, R., Kim, J.J., Lee, M.O., Kim, J., Jung, C.R., Han, T.S., Cho, H.S., Ryu, C.M., and Son, M.Y. (2020). Maturation of human intestinal organoids in vitro facilitates colonization by commensal lactobacilli by reinforcing the mucus layer. FASEB. J. *34*, 9899–9910. https://doi.org/10.1096/fj.202000063R.

Spence, J.R., Mayhew, C.N., Rankin, S.A., Kuhar, M.F., Vallance, J.E., Tolle, K., Hoskins, E.E., Kalinichenko, V.V., Wells, S.I., Zorn, A.M., and Wells, J.M. (2011). Directed differentiation of human pluripotent stem cells into intestinal tissue in vitro. Nature *470*, 105–109. https://doi.org/10.1038/nature09691.

Takebe, T., Sekine, K., Kimura, M., Yoshizawa, E., Ayano, S., Koido, M., Funayama, S., Nakanishi, N., Hisai, T., Kobayashi, T., et al. (2017). Massive and reproducible production of liver buds entirely from human pluripotent stem cells. Cell Rep. *21*, 2661–2670. https://doi.org/10.1016/j.celrep.2017.11.005.

Trisno, S.L., Philo, K.E.D., McCracken, K.W., Catá, E.M., Ruiz-Torres, S., Rankin, S.A., Han, L., Nasr, T., Chaturvedi, P., Rothenberg, M.E., et al. (2018). Esophageal organoids from human pluripotent stem cells delineate Sox2 functions during esophageal specification. Cell Stem Cell *23*, 501–515.e7. https://doi.org/10.1016/j.stem.2018.08.008.

Ungrin, M.D., Joshi, C., Nica, A., Bauwens, C., and Zandstra, P.W. (2008). Reproducible, ultra high-throughput formation of multicellular organization from single cell suspension-derived human embryonic stem cell aggregates. PLoS One *3*, e1565. https://doi.org/10.1371/journal.pone.0001565.

Watson, C.L., Mahe, M.M., Múnera, J., Howell, J.C., Sundaram, N., Poling, H.M., Schweitzer, J.I., Vallance, J.E., Mayhew, C.N., Sun, Y., et al. (2014). An in vivo model of human small intestine using pluripotent stem cells. Nat. Med. *20*, 1310–1314. https://doi.org/10.1038/nm.3737.

Wilson, H.K., Canfield, S.G., Hjortness, M.K., Palecek, S.P., Shusta, E.V., Múnera, J., et al. (2015). Exploring the effects of cell seeding density on the differentiation of human pluripotent stem cells to brain microvascular endothelial cells. Fluids Barriers CNS *12*, 13. https://doi.org/10.1186/s12987-015-0007-9.

Yoshida, S., Miwa, H., Kawachi, T., Kume, S., and Takahashi, K. (2020). Generation of intestinal organoids derived from human pluripotent stem cells for drug testing. Sci. Rep. *10*, 5989. https://doi.org/10.1038/s41598-020-63151-z.